Modeling the free-radical polymerization of hexanediol diacrylate (HDDA): a molecular dynamics and graph theory approach

Torres-Knoop, A.; Kryven, I.; Schamböck, V.; Iedema, P.D.

DOI
10.1039/c8sm00451j

Publication date
2018

Document Version
Author accepted manuscript

Published in
Soft Matter

Soft Matter

Accepted Manuscript

This article can be cited before page numbers have been issued, to do this please use: A. Torres-Knoop, I. Kryven, V. Schamboeck and P. Iedema, *Soft Matter*, 2018, DOI: 10.1039/C8SM00451J.

ROYAL SOCIETY OF CHEMISTRY

rsc.li/soft-matter-journal

View Article Online
DOI: 10.1039/C8SM00451J

Journal Name

ARTICLE TYPE

Cite this: DOI: 10.1039/xxxxxxxxxx

Modeling the free-radical polymerization of hexanediol diacrylate (HDDA): a molecular dynamics and graph theory approach†

Ariana Torres-Knoop*,[a] Ivan Kryven[a], Verena Schamboeck [a] and Piet Iedema[a]

Received Date
Accepted Date

DOI: 10.1039/xxxxxxxxxx

www.rsc.org/journalname

In the printing, coating and ink industries, photocurable systems are becoming increasingly popular and multi-functional acrylates are one of the most commonly used monomers due to their high reactivity (fast curing). In this paper, we use molecular dynamics and graph theory tools to investigate the thermo-mechanical properties and topology of hexanediol diacrylate (HDDA) polymer networks. The gel point was determined as the point where a giant component was formed. For the conditions of our simulations, we found the gel point to be around 0.18 bond conversion. A detailed analysis of the network topology showed, unexpectedly, that the flexibility of the HDDA molecules plays an important role in increasing the conversion of double bonds, while delaying the gel point. This is due to a back-biting type of reaction mechanism that promotes the formation of small cycles. The glass transition temperature for several degrees of curing was obtained from the change in the thermal expansion coefficient. For a bond conversion close to experimental values we obtained a glass transition temperature around 400 K. For the same bond conversion we estimate a Young's modulus of 3 GPa. Both of these values are in good agreement with experiments.

1 Introduction

The understanding of polymer networks has attracted attention from several fields for many years. Solid polymer networks emerge from the polymerization of liquid monomers with more than two reactive groups. Coatings, resins and even old oil paint are examples of polymer networks with an enormous impact in many segments of society.

In the last years, light induced polymerization techniques (photocurable systems) have gained popularity over thermally induced polymerization techniques (thermocurable systems) because (1) the polymerization process itself is more energy efficient, (2) photocurable systems are more sustainable (systems are entirely composed of reactive components and therefore no volatile organic components are involved and no organic solvents are needed) and (3) they are one of the most efficient methods to achieve a high degree of curing[1]. In addition, light induced polymerization can also be used to control specific properties in the product materials, for example, by the use of lasers or by using exposure with masks to create patterns[2].

An important class of photocurable systems are based on free-radical polymerization[3]. This type of polymerization is characterized by a sequence of reactions: *initiation*, *propagation* and *termination* that ultimately result in the formation of large polymer molecules and eventually a polymer network (gelation). Initiators start the propagation reactions (I•+R→R•), where the macroradicals R•react with unreacted vinyl groups (either pending from the polymer or in free monomers). A polymeric network is formed as these pending vinyl groups undergo crosslinking reactions with propagating radical sites. The polymerization process ends with the reactions between radicals and macroradicals via combination (R_n•+R_m•→ R_{n+m}) or disproportionation (R_n•+ R_m•→ R_n+R_m).

The physical properties of the photocurable systems are mostly determined by the type of monomer(s) used, *e.g.* their reactivity, polymerizable group and functionality (the number of polymerizable groups per monomer). Monomers with acrylate functional groups have become standard because of their high reactivity (acrylates>methacrylates>vinyl>allylic)[4] and due to their availability in a wide range of functionalities. However, despite their increasing importance, little is known about the molecular structure and topology of the polymer networks they form and their influence in the properties of the product material.

The creation of solid polymer networks starting from liquid monomers is a challenging topic for modelers. The complex issue of kinetic rates drastically decreasing because of the reduc-

[a] Van 't Hoff Institute for Molecular Sciences, University of Amsterdam, Science Park 904, 1098 XH Amsterdam, The Netherlands; E-mail: A.TorresKnoop@uva.nl

View Article Online
DOI: 10.1039/C8SM00451J

ing mobility of the functional groups, finally becoming diffusion controlled, is still far from being solved. Even more, due to the extremely varying reaction conditions in photocuring, the usual concepts of kinetic modeling in terms of concentrations of reactive species and rate coefficients might no longer apply. Knowing how the polymer networks evolve during polymerization is expected to assist the understanding of polymerization kinetics. Experimentally, the speed of the process and the complexity of the networks makes them difficult to characterize. The topology of the networks, on which the physical properties ultimately depend on, are only scarcely experimentally accessible.

Molecular simulations provide a link between the molecular-level characteristics of the system and its properties, either observable properties like a gel point or physical properties like elasticity. Thus, they can contribute to a better understanding on the kinetics, network evolution and properties of polymer network, eventually leading to guidelines for the design of new polymer-based materials[5].

The current state-of-the-art of molecular simulations does not allow a straightforward application of concepts regarding polymer networks. Generating crosslinked structures using molecular simulations is an inherently complex problem, since chemical reactions are not part of the Hamiltonian mechanics that drive classical Molecular Dynamics (MD). There is no general solution for how to create bonds and no standard protocol for the generation of network models. This has lead to the development of several 'Reactive Molecular Dynamics' approaches to model chemical bonding. Farah *et al.*[6] classified the reactive approaches as based on (1) empirical reactive force fields and (2) on a cutoff criteria. In the first approach, the force fields are designed to model the bonds formation by using switching functions to model a continuous transition from reactants to products. They aim to reproduce some reaction kinetics as well as to model the transition state geometries. Examples of these types of force fields are the Empirical Valance Bonding force field[7](EVB), ReaxFF[8] and AIREBO[9]. A good review of these force fields is given by Hartke and Grimme[10]. In the second approach, which is still the most commonly used to either prepare systems for further simulations or to study generic aspects of the polymer networks, bonds are created when predefined atoms (reactive sites) are spatially close. The bond formation can be done in a single-step (static) or in multiple-steps (dynamic)[11]. In the single-step approach the reactive sites are kept fixed and Monte Carlo simulations are used to identify the bonds of minimal aggregate length[12,13]. In the multiple-step approach, the diffusion of monomers is fully simulated using MD and the reaction criteria is checked at regular times[14–19]. Jang and Sirk[11] compared the properties of the fully cured polymer networks formed by the two methods (single-step and multiple-step) and found that the only relevant difference is in the distribution of molecular weights. For both of these approaches, static and dynamic, several protocols mixing reaction and relaxation steps have been proposed in literature that successfully reproduce experimental data such as the density, viscosity, glass transition and volume shrinkage. Khare and Khare[18,19] used a rather large fixed reactive radius, but varied the force constant of the bond to avoid large jumps in the energy. They alternated this process with MD simulations to ensure the system was relaxed. Demir and Walsh[20] adopted a similar approach to study crosslinked EPON-862/DETDA, but using an increasingly larger capture radius during the simulations to achieve high conversion. They also presented a protocol to consider the charge changes during the chemical reactions. Xu and Wu[14] studied the polymerization of epoxy resins DGEBA and IPD(isophorone diamine) with a similar protocol, but using a combination of several steps of MD and minimizations for the relaxation of the system. Li and Stratchan[16] and Li *et al.*[21] proposed a multi-step relaxation process to study crosslinked EPON-862 and DETDA. Heine *et al.*[22] used modified bond potentials (harmonic at close range and linear at longer distances) to study the curing of poly(dimethylsiloxane). Varshney *et al.*[15] used a variable capture radius to simulated the curing of epoxy resins and, in between bonds formation, they used NPT molecular dynamics to relax the structure.

Most of the atomistic modeling of crosslinked polymers using a cut off criteria focus on epoxy resins made by step polymerization. Until now, little has been done in systems that undergo free-radical polymerization. Doherty *et. al*[23] studied the networks formed with TEGMDA and Bis-GMA, a common dental resin composition. Jang *et al.*[17] studied vinyl ester resins and Farah *et al*[24] studied the polymerization of styrene. Free-radical polymerization (chain-growth) is inherently different from step polymerization (bimolecular reactions). In step-polymerization any two molecular species in the system can react. This leads to a polymerization process where the reactions proceed rapidly at the beginning but the overall molecular weight increases slowly (gelation occurs at high conversion). In chain-growth polymerizations, the monomers can only react with the reactive groups. The concentration of monomers decreases steadily with time and a high-molecular-weight is achieved at low conversions[25]. These differences imply a different nature of the MD simulations as well. The 'reactive site' propagation has to be simulated and most of the reactions occur after gelation, at which point the mobility of the system is hampered due to the existence of a 'giant' molecule.

In this work, we expand the applicability of MD simulations to study systems that undergo free-radical polymerization by investigating the evolution of the polymer network of hexanediol diacrylate (HDDA). HDDA is a difunctional monomer characterized by high transparency and low viscosity used in the printing, paint and coating industries mostly as a reactive component to accelerate curing, to improve adhesion, hardness, abrasion and heat resistance. We present a simulation and analysis protocol combining MD simulations and graph theory tools that aim to give insight in the polymerization process and the resulting network properties.

2 Methodology

2.1 Model and system set-up

The HDDA molecules were modeled at a united-atom (UA) coarse-grained level. In Figure 1 the structure of a HDDA molecule and its united-atom representation are shown. We choose the TraPPE-UA force field by Maerzke *et al.*[26] for acrylates, but with a harmonic potential to represent the bonds (as opposed

View Article Online
DOI: 10.1039/C8SM00451J

to rigid bonds). This is necessary for the crosslinking simulations. A summary of the force field functional form and parameters used are presented in Tables 1-4 in the Electronic Supporting Information (ESI).

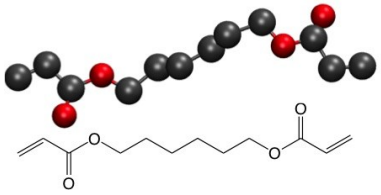

Fig. 1 United-atom representation of 1,6-hexanediol diacrylate (HDDA) molecule. Hydrogens are grouped together with their neighboring carbons.

The initial systems were set up by randomly packing 2000 molecules of HDDA in a 3D periodic simulation cell (initial size 200×200 Å). The systems were then equilibrated in the NVT ensemble at 600 K for 10 ps using a time step of 0.1 fs and further equilibrated at 600 K for 500 ps in the NPT ensemble with a time step of 1 fs. This resulted in simulation boxes of sizes around 100×100 Å. All simulations were carried out using the Nosé-Hoover thermostat[27,28] with a coupling constant of 1 ps and in the constant pressure cases using the Martyna-Tuckerman barostat[29].

2.2 Liquid properties

To study the properties of the liquid monomers at ambient conditions and validate the force field chosen, the equilibrated systems at 600 K were cooled down using the NPT ensemble from 600 K to 300 K and further equilibrated for 500 ps at 300 K. The equilibrated systems at 300 K were then used as input for longer simulations at 300 K in the NVT ensemble to determine the density, self-diffusivity and the viscosity of the system. For the viscosity, a correlation time of 1 ns was used and the simulations were run for 500 ns.

2.3 Curing simulations

The curing of HDDA into a polymer (pHDDA) was done using a cutoff criteria to generate the covalent bonds. In this method, initial reactive radical sites as well as post reactive rules have to be specified. The curing of HDDA involves the saturation of the carbons in the acrylate functional groups. Using the cutoff criteria with the united-atom model, this reaction can be represented by three consecutive steps: (1) the addition of a bond to the carbon that undergoes a reaction, (2) the change of the carbon character from unsaturated to saturated to prevent it from participating in future reactions, and (3) the propagation/regeneration of the reactive site by changing the character of the neighboring carbon from unsaturated to reactive. A summary of the main reactions and their representation using the UA-model is given in Figure 2. Figure S1, shows a polymer network of HDDA after curing simulations.

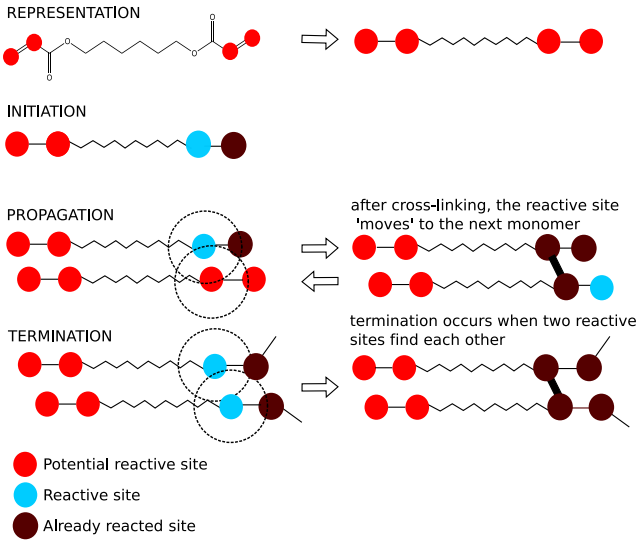

Fig. 2 HDDA molecules are represented as composed by four possible reactive sites. Initiation is represented by including in the system at the beginning of the simulation monomers with one reactive site (radical). Propagation occurs when a reactive site is in the proximity of a possible reactive site. Termination by combination occurs when a reactive site is in the proximity of an other reactive site. Both carbons in the vinyl group were assumed as equally reactive.

2.4 Properties of the cured networks

The curing simulations were performed in the NPT ensemble at 600 K (to increase the monomers diffusivity and prevent the system of getting trapped in a glassy state). Only propagation and termination by combination were simulated explicitly (acrylates mostly undergo combination reactions[25,30]). The 'initiation' step was simulated by setting a given amount of monomers in their 'reactive' form (see Figure 2). This can be chemically thought of as a system exposed to a short but very intense radiation. We will discuss this artificial condition below.

The cutoff radius for reactions to occur was set to 4 Å. This number was chosen just slightly larger than the van der Waals (VDW) radii of the carbons. A smaller cutoff radius would not allow for the curing process to occur (molecules rarely get closer than their VDW radius) and a larger cutoff could cause severe increase of the strain in the system upon curing. Apart from the cutoff radius, the curing process is regulated by (1) the probability of forming a bond, (2) the checking frequency and (3) the initial amount of monomers set as radicals. An increase in the probability of forming a bond, in the initial amount of monomers set as radicals, in the reaction radius or in the checking frequency, speeds up the conversion of double bonds in the system as a function of simulation time.

For our simulations we used a probability of forming a bond of 0.5 and we set 10 ps as the time for checking the proximity of reactive sites. In general, given the reactivity of radical species, we would expect that if they are in the proximity of each other or in the proximity of a carbon-carbon double bond, the probability of a reaction to take place is 1.0. We chose 0.5 to avoid too many bonds from being created at the beginning of the simula-

View Article Online
DOI: 10.1039/C8SM00451J

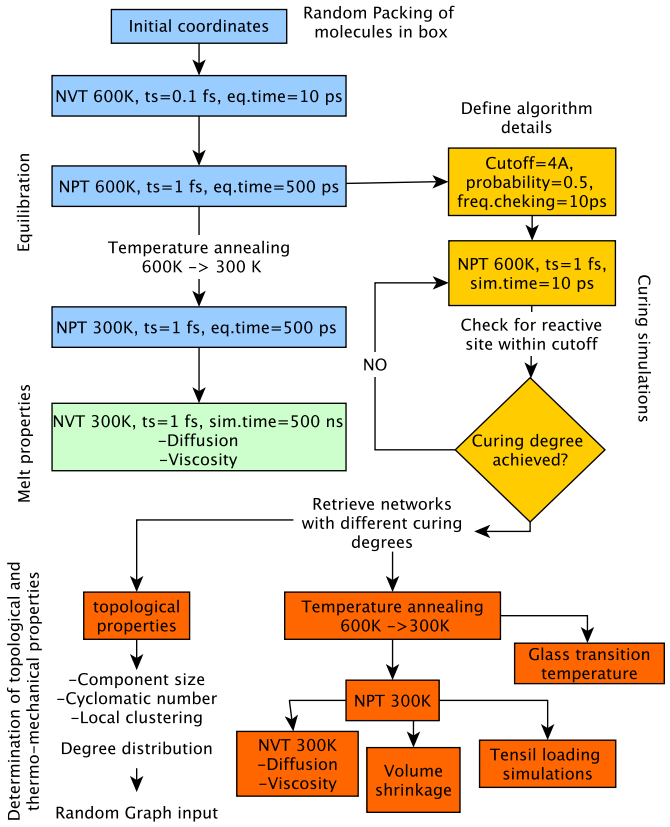

Fig. 3 Simulations performed in this work.

tions and therefore internal stress to be build-up. In real experimental radical polymerization systems the initial concentration of monomer radicals is very low, in the order of 10^{-5} mole/L. In simulations, this situation can not be reproduced without an enormous increase in the simulation time (as the system size has to be very large). Therefore, most of our simulations were performed by setting a reactive radical site in 5% of the monomers. The effect of increasing or decreasing the amount of radicals in the system is analyzed in the next section.

As curing occurs, the chemical reactions cause changes in the thermo-mechanical response of the product material; the increase in molecular weight leads to an increase in viscosity, glass transition temperature and density. Simulations that mimic such processes provide valuable information to understand and ultimately tune processing conditions of thermosets. In order to study such properties, the polymer networks at different degrees of curing were cooled down to 300 K and used as input for further MD simulations. We studied the monomers mobility, volume shrinkage, glass transition and Young's modulus. The self-diffusivity coefficients and viscosities were obtained from NVT simulations at 300 K. The Young's modulus were determined from the initial slope of the stress-strain curve, obtained from non-equilibrium uniaxial-tensile test simulations. The glass transitions were obtained by performing NPT simulations at different temperatures. The systems were cooled down from 600 K to 150 K at a rate of 10 K/100 ps. A summary of the simulations performed can be found in Figure 3. All the simulations in this work were performed using the freely available LAMMPS software package[31].

3 Network formation and gel point

3.1 Network formation

Starting from a liquid solution of 2000 HDDA monomers, 5% of them reactive, we performed eight independent simulations to determine the liquid solution properties and validate our model and force field. The density was estimated to be 1.025 $\pm$ 0.02 kg/m^3 and the viscosity obtained was 3.3 $\pm$ 0.8 cP. The density is in excellent agreement with experimental values[32–34]. The viscosity is slightly underestimated[35], albeit in the right order of magnitude. Note that underestimating viscosity when using united-atom models has already been reported. Maerzke *et al.*[26] reported a deviation of around 20% from the experimental viscosity values for methyl and ethyl acrylate and methyl and ethyl methacrylate. We also computed the self-diffusion coefficient of HDDA molecules in liquid solution and found it to be around 0.3×10^{-5}cm^2/s. This is in good agreement with molecules of similar size and functionality[36,37].

The eight independently equilibrated systems were subsequently subjected to the above described curing simulation conditions until the percentage of reacted functional groups was larger than 90% (Figure S2). A higher bond conversion is difficult to attain as (1) the number of available non-reacted vinyl groups decreases and (2) the mobility of the system slows down dramatically with curing. In Figure 4a the self-diffusion coefficient of the unreacted HDDA molecules as a function of bond conversion (χ) is presented. The bond conversion is defined as the ratio between the already formed covalent bonds in the system and the total number of covalent bond that *can* be formed in the system. The diffusivity of HDDA monomers decreases with increasing conversion at a very fast rate. Groups of already reacted HDDA molecules suffer an even faster reduction of mobility and become basically frozen in space at early stages of the polymerization process. In general, this causes radical trapping and further conversion is difficult to achieve. Trapping of radicals in pHDDA has already been reported before[38]. These authors observed additional conversion after heating the photopolymerized samples in the dark, which they attributed to the remobilization of the trapped radicals. In Figure S3, the bond conversion for different curing temperatures and ensembles is presented. Both of these parameters, temperature and ensemble, have an effect in the mobility of the system by either providing more kinetic energy to the monomers or not allowing the volume to contract with polymerization. A higher mobility indeed promotes higher conversion. Using 300 K as curing temperature does not enable the system to reach experimental conversion values in a reasonable simulation time.

Figure 4b, shows the evolution of the degree of the molecules with conversion. The degree of a molecule is defined as the number of bonds a molecule is engaged in. In the case of HDDA, the maximum possible degree of a molecule is four. Initially, all molecules have degree zero (they are monomers). As polymerization takes place, the monomers become covalently bonded to

View Article Online
DOI: 10.1039/C8SM00451J

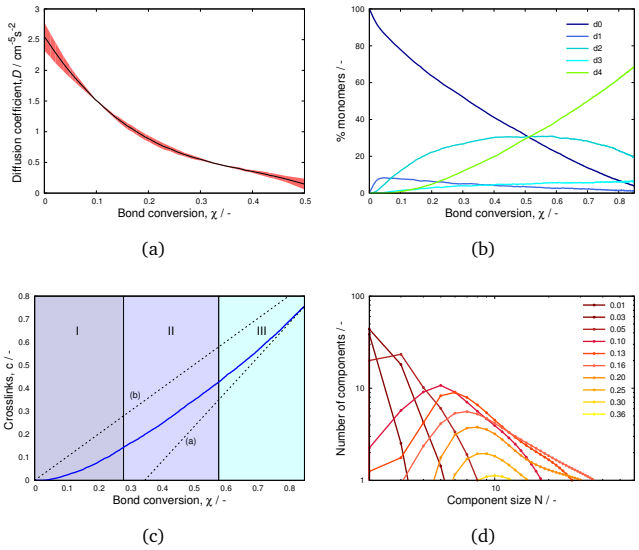

Fig. 4 (a) Diffusion coefficient of the unreacted HDDA molecules as a function of conversion. (b) Monomers degree evolution with conversion. (c) Crosslinks formation evolution with conversion. Black dash lines correspond to a slope of a=1.5 and b=1. (d) Connected components size evolution as a function of conversion.

other molecules giving rise to molecules with degree one, two and eventually three and four. The number of molecules with degree two initially increases but around 0.5 conversion starts to decrease in favour of molecules of degree three and four. This implies that most of the reactions after this conversion value form crosslinks. A crosslink is defined as a monomer connecting two monomer chains (monomer with degree higher than two). Figure 4c shows the relationship between bond conversion and crosslinks formation. We can distinguish three different behaviours. In region I (slope < 1), most bonds are formed between monomers of degree zero and degree one (no crosslinks are formed); this leads to the emergence of some linear segments. In region II (slope ~ 1), most bonds contribute to the formation of one crosslink; at least one of the reacting monomers is a free pendant double bonds (FPDBs). In region III (slope > 1), some bonds contribute to the formation of one or two crosslinks; FPDBs react with each other. In general the behaviour depicted in Figure 4c, reflects a polymerization process where the overall reactivity of the free monomers and the FPDBs are comparable[38]. The black lines represent the extreme cases when (a) free monomers are more reactive and (b) FPDBs are more reactive. Experiments performed by Kloosterboer *et al.*[39], where they monitored the unreacted monomers using High Performance Liquid Chromatography (HPLC) to determine the molality of crosslinks as a function of conversion show a similar behaviour to the data presented in Figure 3c. However, in the experiments by Kloosterboer *et al.*, for conversion values lower than 10%, they found a small kink in the curve of bond conversion versus crosslinks towards the (b) line. This kink suggests that the FPDBs have an even higher reactivity at lower conversions.

In Figure 4d, we present the evolution of the system connected components sizes (excluding the largest connected component and starting from size two to exclude monomers) as a function of bond conversion. We define a connected component as a group of covalently bond monomers. Initially, the connected component size distribution becomes broader and the average connected component size shifts towards larger values. However, between 0.16 and 0.20 bond conversion this trend changes. The distribution becomes narrower. This change in the connected component size distribution is caused by the formation of the giant connected component. The formation of the giant connected component that percolates throughout the entire system is identified as the gel point. Upon further increase of the conversion, the gel or network fraction increases at the expense of the polymer molecules in the 'sol' phase (finite size polymer molecules) and the whole system becomes more solid-like.

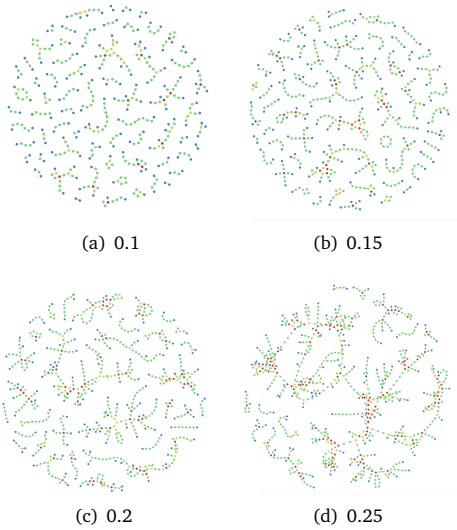

Fig. 5 Topological structure of pHDDA at different conversion values (0.1,0.15,0.2,0.25) before and after the gel point. Each node represents a HDDA molecule and the color of the node represents the degree of the molecule (degree one=blue,degree two=green,degree three=yellow,degree four=red). Before the gel point (top row) there are many molecules of comparable size. After the gel point (bottom row) the largest component dominates the size.

In Figure 5, we present the topological structures of the system for bond conversion values close to the gel point. Each node represents an HDDA molecules. Figure 5a and 5b, just before the gel point, show that at these conversion values the system is still composed of several components where many monomer have only degree one or two. Figure 5c, around the gel point, shows the "collapse" of several of these components into much larger ones. Figure 5d, after the gel point, shows how molecules are connected to each other in a giant component and how the overall degree of the molecules has increase.

Gelation directly affects the mobility of the system but does not inhibit the curing process. In fact, most of the propagation occurs in the gel. This is in agreement with what we observed in Figure 4b and 4c. After the gel point, the curing process mostly increases the crosslink density.

In molecular simulations, we can directly monitor the evolution of the largest component size and estimate the gel point as the

View Article Online
DOI: 10.1039/C8SM00451J

inflection point in the component size of the largest component. This is shown in Figure 6. The inflection point appears around 0.18 bond conversion. In practice, this chemically defined gel point is hard to measure, since the thermo-mechanical properties (e.g. viscosity) only change appreciably after a certain amount of gel is present and the crosslink density of that gel has increased.

The gel point can also be determined as the maximum of the Reduced Molecular Weight (RMW), which is defined as the weight-average molecular weight of all the reacted components except the largest one[40,41] (area under the component size distribution in Figure 4d) . In Figure 6 we show that also the RMW criteria suggests the gel point around 0.18 conversion.

Recently Kryven *et al.*[42] proposed a criteria to estimate the gel point from the degree distribution of the system. The degree distribution d_k denotes the probability that a randomly chose monomer is connected to k other monomers. Using the degree distribution obtained from MD simulations, we found the gel point to be at ∼0.11 bond conversion.

Using the random graph method[42,43](RG), in which the system properties are determined from the mean behaviour of all possible topologies that can be recovered from a given degree distribution, we also obtained the evolution of the largest component size[42–44]. The agreement with the directly monitored largest component from MD is excellent at high conversion but again the gel point is slightly underestimated (Figure 6). In general however, the agreement is remarkable given the significant differences in the approach and assumptions between MD and the random graph model. One of these differences is that random graph method does not account for cycles in the sol phase. As will be discussed below, the occurrence of early cycles delays the gel point.

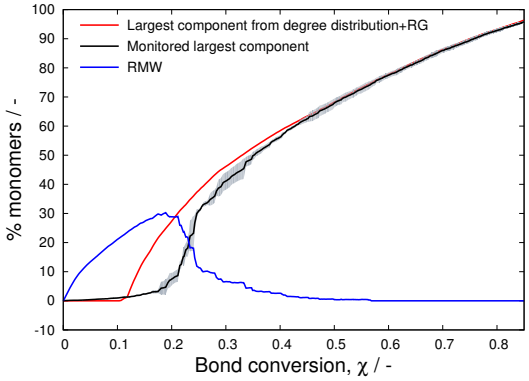

Fig. 6 Largest component evolution as a function of bond conversion. The black line is the largest component monitored from MD simulations. The blue line corresponds to the evolution of the reduce molecular weight. For both cases, the average over eight independent polymerization runs is plotted; the shaded area represents the standard deviation. The red line is the evolution of the largest component determined using the random graph model with the degree distribution obtained from the MD simulations.

The gel point can also be determined from the appearance of secondary cycles (intramolecular reactions within the same component)[15]. The appearance of secondary cycles and the overall changes in the topology of the networks were obtained using graph theory tools.

Figure 7a shows the evolution of the cyclomatic complexity (M) as a function of conversion. The cyclomatic complexity is directly related to the appearance of cycles and is defined as:

$$M = E - N + P,\ M \geq 0 \qquad (1)$$

where E is the number of monomers in the system, N is the number of bonds between monomers and P the amount of components. A positive cyclomatic complexity means that there are cycles in the system. In Figure 7a the cyclomatic complexity as a function of conversion is presented (red line). Cycles are formed at very early stages of the polymerization process. A more detailed analysis of the simulations shows that these early cycles are mostly cycles formed by one or two HDDA molecules (Figure S4) and is only after the gel point that most of the larger cycles start to appear due to crosslinking.

The appearance of small cycles implies that (1) the propagating radical reacts with the unreacted vinyl group in the same molecule (cycles of size one) and (2) FPDBs react with the vinyl group of the first added monomer after they are formed (cycles of size two). Figure 8a illustrates both of these processes. Furthermore, it is immediately clear, that the small cycle reaction is in competition with crosslinking reactions of both the vinyl group and the radical site on the last added monomer. Consequently, strong small cycle formation will delay the onset of gelation, which is caused by crosslinking reactions.

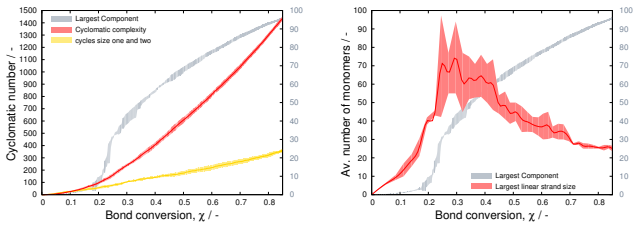

Fig. 7 (a) Cyclomatic complexity as a function of bond conversion. (b) Largest linear strand size (in monomer units) as a function of bond conversion. The largest component evolution is also plotted in both cases for comparison (right axis). The average over the eight independent polymerization runs is ploted; the shaded area represents the standard deviation.

Similar cycles have previously been discussed in literature, but the size of the cycles was not addressed. Dusek and Ilavsy[45] identified FPDB reactions with radicals in the same propagating chain as a dominant reaction of FPDBs at low conversion, but did not specify how far does the radical have to propagate before cyclization is observed. Elliott *et al.*[46] developed a kinetic model where a higher reactivity of the FPDBs with the propagating radical in the same chain was accounted for. With this model, they obtained better agreement with the experimental results by Kloosterboer *et al.*[47] for the fraction of fully reacted monomer units of HDDA as a function of bond conversion. They also found that the FPDBs reactivity is highest when it has 'just been created'.

The flexibility of the molecule strongly determines the reactiv-

View Article Online
DOI: 10.1039/C8SM00451J

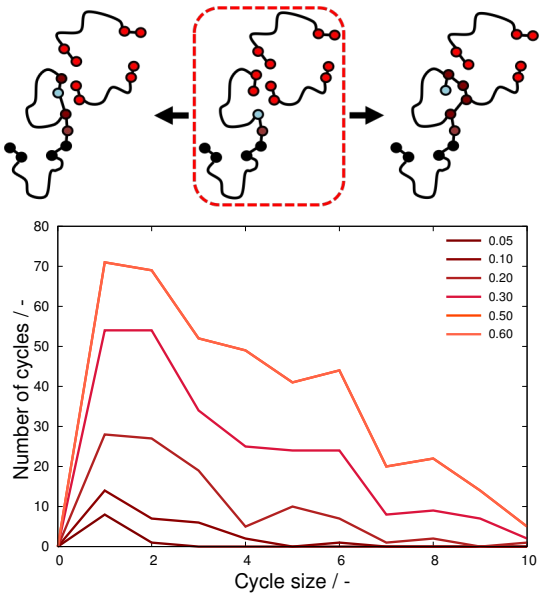

Fig. 8 Top: formation of cycles of size one (left) and (two). Color code: black carbons represents already reacted carbons; blue carbon is the carbon bearing the radical; red carbons represent unreacted carbons. Bottom: cycle size distribution for different bond conversion values. The plot has been cut to cycles of size ten but larger cycles might exist.

ity of the FPDBs with the nearby propagating radicals and in fact determines the size of the cycles that can be formed. In Figure 8b we present the distribution of cycles size (up to ten) for different bond conversion values. For all cases, cycles of size one and two are the most abundant. Hosono *et al.*[48] studied the effect of chain flexibility in the cross-linking process and found that flexible chains first form microgel-like clusters, whereas the rigid chains effectively form the network structure. They attributed this to the enhanced intramolecular reactivity of flexible chains leading to the formation of cycles. In Figure S5 we present the histogram of the end-to-end distance of HDDA in the liquid phase. We observe that in the liquid phase the molecule's are most likely in a semi-coil state, but they can coil and uncoil. A further analysis using metadynamics, shows that the energy barrier of coiling and uncoiling in the liquid phase is between 5-10 kcal/mol (depending on the molecule's environment). This barrier can easily be crossed at 600 K but also at 300 K. Hence, the formation of small cycles is not an artifact from the high curing temperature. Details of the metadynamics simulations can be found in the ESI. Interestingly, these small cycles are created at a similar rate at every stage of the curing process (Figure 7). Dusek *et al.*[49] and Kloosterboer[47] previously theorized a decrease in reactivity of the FPDBs with conversion. They hypothesized that the FPDBs are shielded by the polymer network formation from further reacting. For cycles of size one and two this effect seems to be negligible. Importantly, even though the FPDBs reactivity is enhanced due to the molecule's flexibility, most reactions take place with free monomer due to their large concentration. Only about 5% of the bonds between vinyl groups lead to the formation of cycles of size one and about 10% lead to the formation of cycles of size two.

In a network several paths exist between any two nodes, but there is a shortest path. Figure 7b shows the average largest shortest path in the network as a function of conversion. This quantity initially increases as larger clusters are formed; it reaches a maximum close to the gel point and it decreases after the gel point due to the formation of crosslinks. Close to full conversion, the largest shortest path between monomers is roughly the ratio of the simulation box size and the average monomer length.

4 Effect of initial amount of 'radical concentration' on the polymer network topology

In order to understand the effect of the initial concentration of reactive monomers, we performed simulations with different concentrations ranging from 1-10%. In Figure S6, the bond conversion as a function of simulation time is presented. The amount of 'radicals' in the system determines the rate and degree of curing. Sarkar *et. al*[50] studied the polymerization of mixtures of BisGMA and TEGDMA (70:30) with three different light intensities (100,500,2000 mW/cm^2). The light intensity determines the amount of radicals present in the system. They found a similar trend for the evolution of the degree of conversion with time as a function of 'radicals' concentration. They also reported that the relaxation time of the system increases with conversion (due to gelation). Even more, they showed that the increase in the relaxation time occurs at higher conversion values with increasing light intensity. Figure 9a, shows that the increase in the amount of 'radicals' in the system delays the gel point and sharpens the inflection that determines it. This result is in agreement with the experiments by Sarkar *et. al*. This finding is also in line with the fact that in linear radical polymerization smaller initiator concentrations lead to longer chains. Okay[51] reports a similar result for crosslinking polymerization. Li *et al.*[52] also provide experimental evidence for a system were increasing the amount of chain transfer agent, which reduces the size of sol molecules as similar as increasing initiator concentration, does indeed delay the gel point.

Increasing the amount of initial reactive molecules in the system makes the system resemble more to a step polymerization. Note that for step polymerization Flory's gelation theory[53] predicts a gel point at $1/(f-1)$, where f is the maximum degree of the monomers. For the case of HDDA, this implies a gel point at 0.33, which seems the asymptotic limit for increasing radical concentration in Figure 9a. At conversion values near the experimental end conversion (around 78-85% Iedema *et al*[3]), the largest component size is basically independent of the initial concentration of reactive monomers.

In Figure 9b, we present the cyclomatic complexity for different initial reactive monomers concentrations. For all concentrations, the rate of cycles formation increases with conversion. However, the increase of cycles is more noticeable and occurs at higher conversion values with increasing radical concentrations. The point of the sudden speed up of cycles formation is in agreement with the gel formation. In Figure 9c, the evolution of small cycles is presented. Again, the rate of small cycles formation with bond conversion depends on the initial concentration of reactive

View Article Online
DOI: 10.1039/C8SM00451J

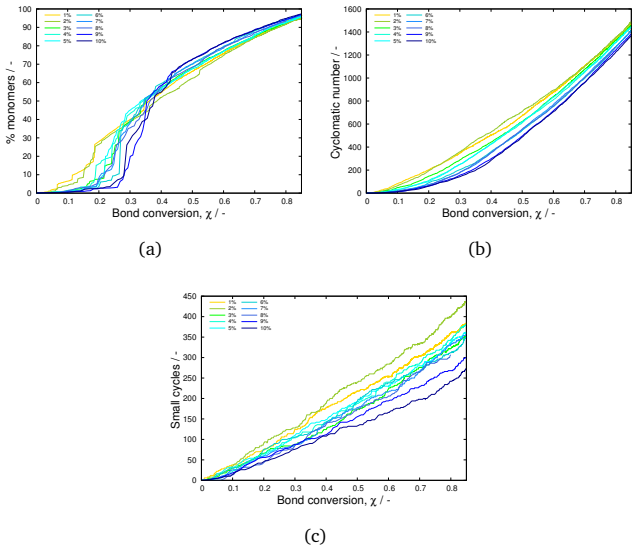

Fig. 9 (a) Largest component size evolution, (b) cyclomatic complexity and (c) small cycles for different amounts of initial reactive monomers as a function of conversion.

monomers. Regarding the evolution of the monomers degree (Figure S7), the main differences are observed for the monomers with degree one and degree three. A monomer can only have degree one when (1) it is an initial reactive monomer with the other vinyl group still unreacted and (2) it is bearing a radical at the end of a polymer chain with the other vinyl group still unreacted. Therefore, it is not surprising that their concentration is directly related to the initial amount of reactive monomers. Monomers of degree three appear when both vinyl groups have undergo some reaction. For most monomers, degree three is a short lived state. As polymerization continues, they become degree four. This is not the case for the initial reactive monomers which, by definition, can only be involved in three bonds. If we assume full conversion, the concentration of monomers with degree three will be equal to the initial amount of reactive monomers and the concentration of monomer with degree four will be equal to the total number of monomers minus the number of initial reactive monomers.

An other important difference between our simulations an experiments lies in the time frame within which radicals are created. In real photopolymerization, systems are exposed to radiation during the whole curing process, which continuously generates free radical monomers. Here, we have created a fixed amount of 'radical monomers' at the beginning, which represents the scenario of a very short but intense radiation. The main difference between these cases is that, when radicals are continuously created, radical sites tend to be more present in recently initiated monomers than in the giant component, so that the population of molecules with radicals have a higher mobility on average. Our preliminary attempts to simulate initiation and steady state conditions show that, although there are several differences in the network topology at low conversion values, at experimental conversion values these differences are very small.

5 Volume shrinkage

During network formation volume shrinkage occurs (1) because the larger van der Waals intermolecular spacings are replaced by smaller intramolecular covalent bonds, and (2) because of the different change in entropy and free volumes related with the packing efficiency of the system. Experimentally, the volumetric shrinkage is difficult to determine because most measurements using pressure-volume-temperature analysis (PVT) also include the effects of thermal expansion. In molecular simulations, the volumetric shrinkage can be obtained by equilibrating in the NPT ensemble the systems at different degrees of curing. Figure 10 shows the average volumetric shrinkage as a function of conversion obtained for pHDDA. For acrylates, based on the experimental volume change per mole of 22.5 cm^3/mol[54], a volume shrinkage of about 10% can be expected[55]. Ji *et. al*[56] used reflective laser scanning to measure the volume shrinkage of pHDDA for different temperatures and initiator concentrations and found that for a temperature of 20 °C close to 0.8 conversion, the volume shrinkage was 16 ± 0.5 %. Both, the theoretical estimate and the experimentally determined values, are in good agreement with our results. Interestingly, the volume seems to expand again after 0.75 bond conversion albeit a much larger standard deviation. This larger standard deviation bar is probably caused by the large internal stress in the structure at high conversion values.

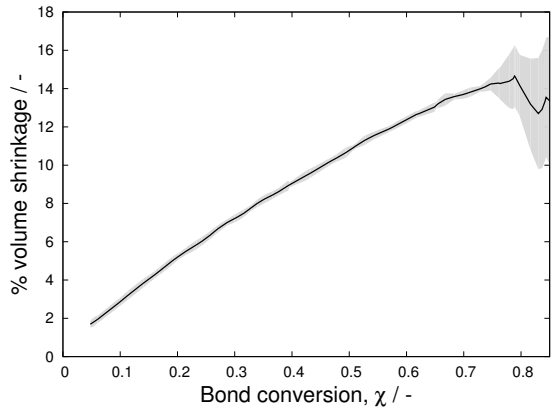

Fig. 10 Volume shrinkage as a function of bond conversion. For each bond conversion, the volume was obtained from the average of 1 ns at 300 K in the NPT ensemble. The average over the eight independent polymerization runs is plotted; the shaded area represents the standard deviation.

6 Thermo-mechanical properties

6.1 Glass Transition

The glass transition temperature (T_g) is a property governed by local dynamics and is an intrinsic signature of the molecular structure. Below T_g the motion of the polymer segments dramatically slows down and the mechanical properties of polymers become very different from those above it. Thus, T_g is a key property to determine processing and application temperature ranges for a specific polymer. Several thermodynamic properties, including density (or specific volume), internal energy and specific entropy,

View Article Online
DOI: 10.1039/C8SM00451J

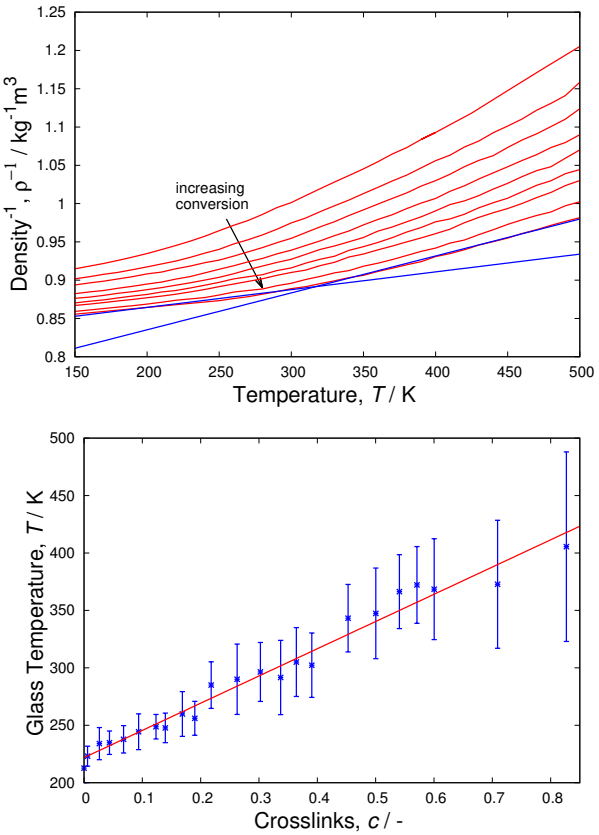

Fig. 11 (a) Inverse density variation with temperature for different degrees of bond conversion (red lines). For each bond conversion, the glass transition temperature can be obtained as the point where the slope of the curve changes (blue lines). (b) Glass transition temperature as a function of bond conversion. The average over the eight independent polymerization runs is plotted; the error bars represent the standard deviation.

can be used in molecular simulations to determine T_g. An abrupt change in the temperature dependence of any of these properties indicates the polymer cannot maintain its equilibrium state anymore and therefore it undergoes a phase transformation into a glassy state. Figure 11a, shows the variation of the inverse density as a function of temperature for different degrees of bond conversion. The glass transition temperature is obtain as the point where there is a change in the slope of these curves. The change in slopes becomes less obvious with increasing conversion due to the mobility loss in the system. This has previously been observed for pHDDA and other highly crosslinked systems[57]. Figure 11b, shows the glass transition temperature as a function of crosslinks. The glass transition temperature for each degree of crosslinking was determined as the point where the slope of the inverse density vs temperature changes (intersection of blue lines in Figure 11a). For a conversion of around 0.8, we found a glass transition temperature close to 400 K. Goswami *et. al*[58] determined the glass transition of pHDDA to be 359 K by using Dynamical Mechanical Analysis (DMA) and to be 328 K by using Thermo-Mechanical Analysis (TMA). It is well known that the glass transition temperature expected from molecular simulations can be higher than the experimentally observed one because the glass transition is a kinetic phenomenon and therefore depends on the cooling/heating rate. An increase of 3 K can be expected per order of magnitude increase in rate[59]. In experiments, one normally monitors the properties to determine T_g over seconds, and these different cooling rates cause the T_g to vary in the order of 5-10 K[60]. However in simulations, the total cooling is done in the order of nanoseconds[61]. Here, we used a cooling rate of 5×10^{-9} K/s. This suggests that the T_g we obtained from the simulations might overestimate the experimentally reported values by around 30 K. Under these assumptions, we get very good agreement between simulations and experiments.

6.2 Young's modulus

The mechanical properties of a material describe how it responds under a certain loading condition. The mechanical properties of polymers are decisive for their applicability, and the degradation of these properties establishes their lifetime in service. The most common mechanical properties to determine in a polymer network include the Young's modulus, Poisson's ratio, toughness ratio, yield strength, fracture strength, and toughness. For all of these properties, the underlying molecular network and topology play a critical role. Here we focus only on the Young's modulus. The Young's modulus describes a material elastic response to small deformations.

To determine the Youngs's modulus, we performed uniaxial tension loading simulations by increasing the length of the simulation cell along the loading direction at every MD step while maintaining atmospheric pressure in the transverse directions using a barostat. The limit of the longitudinal strain was set to be 50%, and the strain rate was set to be $1 \times 10^9\ s^{-1}$. The deformation was carried out according to $L(t) = L_0 \times \exp(\text{rate} \times dt)$, where L_0 is the initial length of the system in the dimension that is being elongated. In Figure 12 the Young's modulus for different degrees of crosslinking is presented (blue data point). For a crosslink density close to experimental values, we found a value of the Young's modulus of around 3-4 GPa. This value is in agreement with other diacrylates or similar molecules. Moraes *et al.*[62] found the Youngs's modulus for different mixtures of TEGDMA, Bis-GMA and Bis-EMA to be between 1-3 GPa. Emami *et al*[63] found the Young's modulus of TEGDMA to be 2.37 GPa and for bisGMA to be 4.15 GPa.

Goswami *et al.*[58] determined the elastic modulus of pHDDA by micro-identation analysis the elastic modulus of pHDDA to be 0.920 ± 0.030 GPa. Using an alternative method, tensil stress experiments, they found the tensil modulus to be 0.464 ± 0.035 GPa at 1% strain. The experiments were carried out at room temperature, but the degree of conversion is not reported.

The Young's modulus depends on the number of crosslinks, degree of the crosslinks and the stiffness of the chain segments between crosslinks. The elastic modulus is generally accepted to be proportional to the crosslinking density, though the prefactor is still controversial. Li and Strachan[64] reported an almost linear increase in tensile modulus with conversion degree for a thermoset EPON82/DTDA. Here, is also appear that the Young's modulus increases linearly with crosslinks. According to De Gennes[65], the

View Article Online
DOI: 10.1039/C8SM00451J

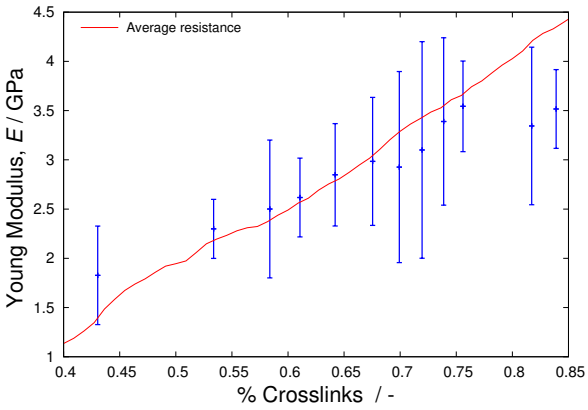

Fig. 12 Young's modulus for different amounts of crosslinks in the polymer network. The overall trend suggest a linear increase of the Young's modulus with crosslinks. The average resistance of the network (red line) captures the overall increase of the Young's modulus with crosslinks very good. In both cases, the average over the eight independent polymerization runs is plotted; the error bars represent the standard deviation.

average resistance distance in the connectivity graph of a polymer plays a definitive role in determining the elastic modulus of the corresponding material. In Figure 12, we compare the Young's modulus obtained from MD simulations with the one computed from the average resistance of the connectivity graph as a function of crosslinks (red line). The behaviour is in very good agreement. More on how the elastic modulus is obtained from the connectivity graph can be found in the ESI.

7 Conclusion

pHDDA networks were successfully generated using molecular dynamics simulations. The obtained thermo-mechanical properties at experimental conversion values are in good agreement with experimental values. The use of graph theory tools allowed us to understand the effects of the molecules flexibility as well as the radical concentration in the networks formation. The formation of small loops, due to the molecules flexibility, plays a crucial role in delaying the gel point. The formation of a gel does not inhibit the formation of small loops. This suggests that the reactivity of FPDBs just after they are made is not hampered during the curing process. This however, does not imply that their reactivity is not affected when dealing with larger macroradicals. The cycle size distribution can provide information on the flexibility of the monomers and monomer chains. As compared to other systems, here every small loops is elastically active due to the high degree of acrylate monomers. We observe a linear relationship between crosslinks and the glass temperature. We also observed a linear relationship between crosslinks and the Young's modulus which we are able to relate (up to a constant) with the resistance of the network.

Acknowledgements

The authors would like to thank the financial support from the Netherlands Organisation for Scientific Research (NWO) via the PREDAGIO project. I.K. acknowledges support from NWO via the research program Veni with project number 639.071.511. V. S. thanks the financial supported by Océ Technologies B.V. and the Technology Foundation STW.

Notes and references

1 J. H. Lee, R. K. Prud'homme and I. A. Aksay, *J. Mater. Res.*, 2011, **16**, 3536–3544.
2 S. Biria and I. D. Hosein, *ACS Appl. Mater. Inter.*, 2018, **10**, 3094–3105.
3 P. Iedema, V. Schamboeck, H. Boonen, J. Koskamp, S. Schellekens and R. Willemse, *Chem. Eng. Sci.*, 2018, **176**, 491–502.
4 C. Barner-Kowollik, P. Vana and T. P. Davis, in *Handbook of Radical Polymerization*, ed. K. Matyjaszewski and T. P. David, John-Wiley and Sons, Inc., USA, 2002, pp. 187–262.
5 V. G. Mavrantzas, *Rheology Reviews*, 2007, 1–52.
6 K. Farah, F. Müller-Plathe and M. C. Bohm, *ChemPhysChem*, 2012, **13**, 1127–1151.
7 A. Warshel and R. M. Weiss, *J. Am. Chem. Soc.*, 1980, **102**, 6218–6226.
8 K. Chenoweth, A. C. T. van Duin and W. A. Goddard, *J. Phys. Chem. A*, 2008, **112**, 1040–1053.
9 S. J. Stuart, A. B. Tutein and J. A. Harrison, *J. Chem. Phys.*, 2000, **112**, 6472–6486.
10 B. Hartke and S. Grimme, *Phys. Chem. Chem. Phys.*, 2015, **17**, 16715–16718.
11 C. Jang, T. W. Sirk, J. W. Andelzm and C. F. Abrams, *Macromol. Theor. Simul.*, 2015, **24**, 260–270.
12 I. Yarovsky and E. Evans, *Polymer*, 2002, **43**, 963–969.
13 P.-H. Lin and R. Khare, *Macromolecules*, 2009, **42**, 4319–4327.
14 C. Wu and W. Xu, *Polymer*, 2006, **47**, 6004–6009.
15 V. Varshney, S. S. Patnaik, A. K. Roy and B. L. Farmer, *Macromolecules*, 2008, **41**, 6837–6842.
16 C. Li and A. Strachan, *Polymer*, 2010, **51**, 6058–6070.
17 C. Jang, T. . Lacy, S. R. Gwaltney, H. Toghuanu and C. U. P. Jr, *Macromolecules*, 2012, **45**, 4876–4885.
18 K. Khare and R. Khare, *Macromol. Theor. Simul.*, 2012, **21**, 322–327.
19 K. S. Khare and R. Khare, *J. Phys. Chem. B*, 2013, **117**, 7444–7454.
20 B. Demir and T. R. Walsh, *Soft Matter*, 2016, **12**, 2453,2474.
21 C. Li, E. Coons and A. Strachan, *Acta Mech.*, 2014, **225**, 1187–1196.
22 D. R. Heine, G. S. Grest, C. D. Lorenz, M. Tsige and M. Stevens, *Macromolecules*, 2004, **37**, 3857–3864.
23 D. C. Doherty, B. N. Holmes, P. Leung and R. B. Ross, *Comp. and Theor. Polymer Science*, 1998, **8**, 169–167.
24 K. Farah, H. A. Karimi-Varzaneh, F. Müller-Plathe and M. C. Bohm, *J. Phys. Chem. B*, 2010, **114**, 13656–13666.
25 G. Odian, *Principles of Polymerization*, John Wiley and Sons, Inc., USA, 4th edn., 2004.
26 K. A. Maerzke, N. E. Schultz, R. B. Ross and J. I. Siepmann, *J. Phys. Chem. B*, 2009, **113**, 6415–6425.
27 W. Hoover, A. J. C. Ladd and B. Moran, *Phys. Rev. Lett.*, 1982,

View Article Online
DOI: 10.1039/C8SM00451J

48, 1818–1820.
28 S. Nosé, *J. Chem. Phys.*, 1984, **81**, 511–519.
29 A. Tuckerman, J. Lopez-Rendon and A. Martyna, *J. Phys. A: Math. Gen.*, 2006, **39**, 5629–5651.
30 G. Moad and D. H. Solomon, *The Chemistry of Radical Polymerization*, Elsevier Science, Amsterdam, 2nd edn., 2005.
31 S. Plimpton, *J. Comp. Phys.*, 1995, **17**, 1–19.
32 *CAS DataBase List*, http://www.chemicalbook.com/ChemicalProductProperty_EN_CB1114704.htm, Accessed: 2018-01-22, CAS No. 13048-33-4.
33 *NIST*, http://webbook.nist.gov/cgi/cbook.cgi?ID=13048-33-4&Units=SI, Accessed: 2018-01-22, CAS No. 13048-33-4.
34 *Sigma-Aldrich*, http://www.sigmaaldrich.com/catalog/product/aldrich/246816?lang=en&region=NL, Accessed: 2018-01-22.
35 P. Glöckner, T. J. S. Struck and K. Studer, *Radiation Curing: Coatings and Printing Inks ; Technical Basics, Applications and Trouble Shooting*, Vincentz Network GmbH & Co KG, Germany, 2008.
36 Y. Zhang, V. Richard M and R. W. Pastor, *J. Phys. Chem.*, 1996, **100**, 2652–2660.
37 G. H. Goo, G. Sung, S. H. Lee and T. Chang, *Bull. Korean Chem. Soc.*, 2002, **23**, 1595–1603.
38 J. G. Klooesterboer, G. M. M. V. de Hei and G. F. C. M. Lijten, in *Integration of Fundamental Polymer Science and Technology*, ed. L. A. Kleintjens and P. J. Lemstra, Elsevier, London, 1986, p. 198.
39 J. G. Klooesterboer, G. M. M. V. de Hei and H. M. J. Boots, *Polym. Comm.*, 1984, **25**, 354.
40 W. Y. Chiu and K. C. Cheng, *Macromolecules*, 1994, **27**, 3406–3414.
41 W. Y. Chiu and Y. C. Chen, *Macromolecules*, 2000, **33**, 6672–6684.
42 I. Kryven, *Phys. Rev. E*, 2016, **94**, 012315.
43 I. Kryven, *Phys. Rev. E*, 2017, **95**, 052303.
44 V. Schamboek, I. Kryven and P. D. Iedema, *Macromol. Theor. Simul.*, 2017, **26**, 1700047.
45 K. Dusek and M. Ilavsky, *J. Polym. Sci*, 1975, **53**, 75–88.
46 J. E. Elliott and C. N. Bowman, *Macromolecules*, 1999, **32**, 8621–8628.
47 Network formation by chain crosslinking photopolymerization and its applications in electronics, Berlin, 1988, pp. 1–66.
48 N. Hosono, Y. Masubuchi, G. Furukawa and T. Watanabe, *J. Chem. Phys.*, 2007, **127**, 164905.
49 K. Dusek and K. Spevacek, *Polymer*, 1980, **21**, 750–756.
50 S. Sarkar, P. J. Baker, E. P. Chan, S. Lin-Gibson and M. Y. M. Chiang, *Soft Matter*, 2017, **13**, 3975–3983.
51 O. Okay, *Macromol. Theor. Simul.*, 1994, **3**, 417–426.
52 W. H. Li, A. E. Hamielec and C. M. Crowe, *Polymer*, 1989, **30**, 1513–1517.
53 P. J. Flory, *J. Am. Chem. Soc.*, 1941, **63**, 3083–3090.
54 N. Silikas, A. Al-Kheraif and D. Watts, *Biomaterials*, 2005, **26**, 197–204.
55 K. Kambli, *Ph.D. thesis*, Georgia Institute of Technology, 2009.
56 L. Ji, W. Chang, M. Cui and J. Nie, *J. Photoch. Photobio. A*, 2013, **252**, 216–221.
57 A. Goswami, A. M. Umarji and G. Madras, *J. Appl. Polym. Sci*, 2010, **117**, 2444–2453.
58 A. Goswami, A. M. Umarji and G. Madras, *Polym. Advan. Technol.*, 2012, **23**, 1604–1611.
59 J. D. Ferry, *Viscoelastic properties of polymers*, John Wiley and Sons, Inc., New York, 3rd edn., 1980.
60 A. J. Kovacs, *J. Polym. Sci. Part A*, 1958, **30**, 131–147.
61 J. Han, R. H.Gee and R. H. Boyd, *Macromolecules*, 1994, **27**, 7781–7784.
62 R. R. Moraes, M. A. C. Sinhoreti, L. Correr-Sobrinho, F. A. Oglari, E. Piva and C. L. Petzhold, *J. Biomater. Appl.*, 2008, **24**, 453–473.
63 N. Emami and K. J. Söderholm, *Open Dent. J.*, 2009, **3**, 202–207.
64 C. Li and A. Strachan, *J. Polym. Sci. Pol. Phys.*, 2015, **53**, 103–122.
65 P. G. D. Gennes, *Journal de Physiquei Lettres*, 1976, **37**, 1–2.

View Article Online
DOI: 10.1039/C8SM00451J

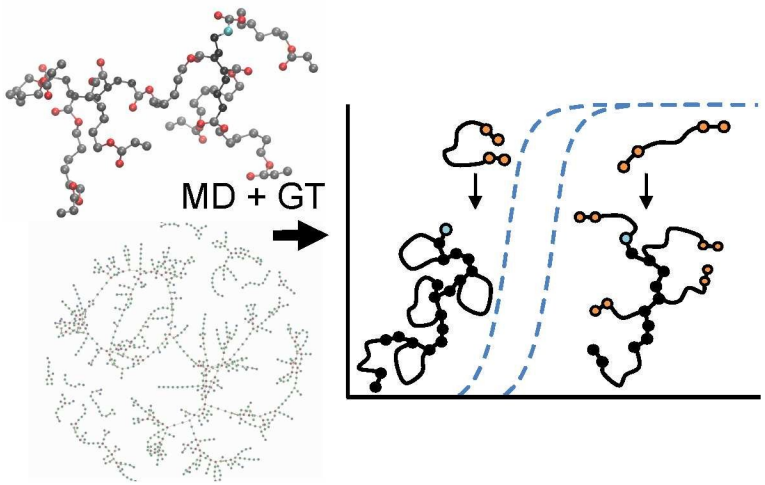

The combination of molecular dynamics simulations and graph theory tools provides important insight into polymerization processes.